Food Chemistry: X 25 (2025) 102146

Contents lists available at ScienceDirect

Food Chemistry: X

journal homepage: www.sciencedirect.com/journal/food-chemistry-x

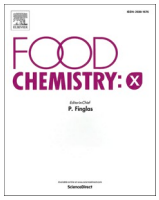

Elucidating the degradation mechanism of beef myofibrillar proteins under hydroxyl radical oxidation through the lens of cysteine oxidation modifications

Jiale Li [a,b], Jun Liu [a,b,*], Hui Yue [a], Yuanyuan Ma [a], He Li [a], Yuanliang Hu [a,b], Xiang Yu [a,b], Weiwei Dong [a], Yanli Feng [a]

[a] Hubei Key Laboratory of Edible Wild Plants Conservation & Utilization, College of Life Sciences, Hubei Normal University, Huangshi 435002, China
[b] Hubei Engineering Research Center of Special Wild Vegetables Breeding and Comprehensive Utilization Technology, Hubei Normal University, Huangshi 435002, China

ARTICLE INFO

Keywords:
Hydroxyl radical
Myofibrillar proteins
Degradation
Redox proteomics
Cysteine sites

ABSTRACT

The study aimed to assess the oxidative modification behavior of bovine myofibrillar proteins (MPs) cysteines (Cys) by hydroxyl radical (·OH) through the construction of an in vitr Fenton reaction system. The ·OH generated by the Fenton reaction induced large-scale oxidative modification of Cys, and redox proteomics identified a total of 1192 differential oxidation sites (Dos), 59 Dos were located in the MPs structure. The Cys of actin (17 Dos), myosin/myomesin (16 Dos), tenascin (12 Dos) and sarcomere (10 Dos) in the MPs structure showed active oxidative modification behavior towards ·OH, especially with the "-C-X-X-X-X-W-" structure amino acid sequence showed high sensitivity. Notably, the oxidative modification of Cys by ·OH was an irreversible process, as evidenced mainly by a significant decrease ($p < 0.05$) in protein sulfhydryl groups and unfolding of protein secondary and tertiary structures. While the intermolecular forces of MPs were altered, with the most direct result being the degradation of MPs, which had a positive effect on beef tenderness and a negative effect on water-holding capacity.

1. Introduction

Protein oxidation inevitably occurs during the refrigeration and production of fresh meat and meat products (Fu, Liu, Zhang, Ben, & Wang, 2020). This is attributed to the oxidation of proteins induced by the external environment of the muscle (light, oxygen, chemicals) and by cellular metabolism (enzymes, metal-catalyzed systems), either directly through reactive oxygen species (ROS), reactive nitrogen species (RNS), or indirectly through the secondary products of oxidative stress (Soladoye, Juárez, Aalhus, Shand, & Estévez, 2015). Among these, ROS is the most classical pathway leading to protein oxidation, which is attributed to its ability to capture hydrogen atoms in proteins to initiate protein oxidation, a process that is considered to be a marker of the onset of protein oxidation (Bao & Ertbjerg, 2019). Extensive studies have been conducted on ROS, which is the term for a collection of oxidatively active substances, including oxygen-containing radicals (e.g., O_2^{-}·, ·OH, ·PO, ·NO) and some non-radical derivatives of oxygen (e.g., H_2O_2, HClO, O_3) (Paulsen & Carroll, 2013). The hydroxyl radical (·OH) is the most reactive oxidant in ROS, and hydrogen peroxide is converted to ·OH by the Fenton reaction in the presence of metal iron ions (Liu, Liu, Zheng, & Ma, 2022). Notably, ·OH production is dependent on iron ions, and it is accurate to say that muscle tissue includes a variety of iron-containing proteins, such as mitochondrial enzymes, hemoglobin, and myoglobin, which serve as substrates for the Fenton reaction through the release of free iron (Lana & Zolla, 2015). These reports indicate that muscle tissue is a carrier of ·OH production, which has a non-negligible effect on meat quality.

ROS represented by ·OH convert oxidative signals into structural modifications by inducing oxidative modifications of muscle tissue myofibrillar proteins (MPs), in particular specific covalent modifications at amino acid sites (Zhang, Yu, You, Xiong, & Liu, 2024). Cysteine (Cys) is the most sensitive amino acid residue to oxidation, and as a candidate amino acid for reversible modification, has a thiol (sulfhydryl) side chain that is highly susceptible to deprotonation under oxidative conditions, and oxidation of the thiols can result in the formation of an intramolecular disulfide bond (S—S) with the adjacent amino acid thiols, or the direct formation of sulfinic acid (S-OH), sulfinic acid (SO_2H), S-nitrosothiols (S-NO) and S-glutathione (S-SG) (Paulsen &

* Corresponding author at: No.11, Cihu Road, Huangshi City 435002, Hubei Province, China.
E-mail address: jliu@hbnu.edu.cn (J. Liu).

https://doi.org/10.1016/j.fochx.2024.102146
Received 14 November 2024; Received in revised form 17 December 2024; Accepted 28 December 2024
Available online 2 January 2025

Carroll, 2013; Sanchez, Riddle, Woo, & Momand, 2008). This oxidative modification alters amino acid side chains, leading to interactions between hydrophilic and hydrophobic regions of the MPs and structural units within muscle segments and between myogenic fibres, affecting protein cross-linking and net protein charge, and thus the structure of muscle fibres and their spatial arrangement (Liu et al., 2022). Such changes in the proteome have been shown to affect quality characteristics, such as color, texture, moisture and digestibility status of meat (Zhang et al., 2024). For example, Oxidation of amino acids in the side chain of proteins induces changes in protein charge and protein aggregation, which reduces protein specific surface area and water holding capacity (WHC) (Xu et al., 2024). Protein oxidation can affect digestibility by modifying amino acids within specific recognition sites of digestive enzymes or by inducing protein cross-linking and aggregation, and that oxidation may also lead to protein unfolding, thereby increasing the accessibility of digestive enzyme-sensitive sites (Zhao et al., 2023).

Given the sensitivity of Cys redox and the importance of its effect on protein structure, it is necessary to resolve the oxidation pattern of Cys in MPs. In the present study, the ·OH was generated by constructing a Fenton system for MPs oxidation treatment to explore the effect of ·OH on protein structure (Li et al., 2021), and hydroxyl radical redox-modified proteins and modified Cys sites were elucidated using redox modification histology and molecular simulation docking techniques. The results of this study may provide valuable information for the quality control of beef during frozen storage.

2. Materials and methods

2.1. Materials and extraction of MPs

The longest dorsal muscles (*M. longissimus lumborum* muscles, loins) from four Chinese yellow cattle [Qinchuan cattle, 18–24 months of feeding age, weighing 400 ± 20 kg (mean ± SD)] were purchased from Yitai Breeding Co., Ltd. (Yinchuan, China). The muscle samples were placed in polyethylene self-sealing bags and subsequently stored in a sampling box filled with ice packs, before being transported to the laboratory for MPs extraction.

Bovine muscle MPs were extracted by referring to the method of Liu et al. (2022) and Xia, Kong, Liu, and Liu (2009) with slight modifications. Briefly, muscle samples with fat and fascia removed were cut into 3 cm × 3 cm × 3 cm blocks. Pre-cooled MPs extraction buffer (4 °C, 0.1 M NaCl, 10 mM NaH_2PO_4, 2 mM $MgCl_2$, and 1 mM EGTA, pH 7.0) (1:4, *g:v*) was added to the muscle and homogenized for 90 s (FJ300-SH Shanghai Standard Model Co., Ltd., Shanghai, China). The homogenate was centrifuged at 2000 ×*g*, 4 °C for 15 min, and the supernatant was discarded to collect the precipitate. The precipitate was added to MPs extraction buffer, homogenized, centrifuged, and washed three times. The homogenate was then filtered through four layers of skimmed gauze, and the pH of the homogenate was adjusted to 6.0 using 0.1 M HCl, and the centrifugation operation was repeated, and the precipitate was muscle tissue MPs.

2.2. Fenton system model of oxidized MPs

MPs were oxidized by the Fenton system. Briefly, the concentration of MPs was adjusted to 50 mg/mL using PBS (containing 0.6 mM NaCl, pH 6.0). The oxidation system was set up as follows: 10 μM $FeCl_3$, 10 μM ascorbic acid, 0, 0.5, 1, 5, 10, and 20 mM H_2O_2, and the oxidation reaction was terminated with 1 mM EDTA after incubation at 4 °C in the dark for 24 h. The oxidized reactants were centrifuged at 2000 ×*g*, 4 °C for 15 min, the supernatant was removed, and the precipitate was washed twice with a 4-fold volume of 15 mM PBS (pH 7.0) (Li et al., 2021; Yu et al., 2024; Zhang et al., 2024).

2.3. Myofibrillar fragmentation index (MFI) and water distribution

The concentration of MPs was adjusted to 0.5 mg/mL and the absorbance was measured at 540 nm using a UV spectrophotometer (Model T6, General Instrument Co., Ltd., Beijing, China), and the MFI was expressed as the absorbance multiplied by 200 (Fan, Gao, Li, Pan, & Zhou, 2024). The distribution of water in MPs was determined using low-field nuclear magnetic resonance (LF-NMR) with reference to our previous report (Liu, Hu, Liu, Zheng, & Ma, 2023). The centrifugal loss of MPs was determined using centrifugation to express the MPs water loss rate, 1.80 ± 0.10 g of MP was placed in a 2 mL centrifuge tube and centrifuged at 4500 ×*g*, 4 °C for 10 min, and the supernatant was collected and weighed. The MPs centrifugal loss was calculated by using the following formula:

$$\text{Centrifugal loss}\ (\%) = \frac{m_2 - m_3}{m_1} \times 100\%$$

where, m_1 denotes the mass of MPs, m_2 denotes the mass of the centrifuge tube and MPs before centrifugation; m_3 denotes the mass of the centrifuge tube and MPs after centrifugation.

2.4. Physicochemical characteristics of MPs

2.4.1. Oxidation of MPs

Briefly, 1.00 g of MPs was added with 9 mL of saline (1:9, *m/v*), mechanically homogenized under ice-water bath conditions for 90 s (Model T6, General Instrument Co., Ltd., Beijing, China), centrifuged at 2000 ×*g* for 10 min, and the supernatant was taken to determine the contents of carbonyl groups and total sulfhydryl groups in the MPs using a kit (Nanjing Jiancheng Bioengineering Institute, Nanjing, China).

2.4.2. Sodium dodecyl sulfate polyacrylamide gel electrophoresis (SDS-PAGE)

The sample volume of MPs and Markers (15–250 kDa) was 10 μL. The electrophoresis instrument (Bio-Rad, CA, USA) parameters were set at voltage 100 V, current 80 mA, 5 % upper concentrated gel, and 12.5 % lower separated gel. At the end of electrophoresis, the staining solution (0.125 g of Coomassie Brilliant Blue R-250, 30 mL of methanol, 10 mL of glacial acetic acid, and 60 mL of ultrapure water) was shaken and stained for 60 min. Subsequently, destaining was performed by oscillation using destaining solution (staining solution without Coomassie Brilliant Blue R-250) until the target protein bands were clearly visible (Xia et al., 2009).

2.4.3. Fourier transform infrared spectroscopy (FTIR)

The concentration of MPs solution was diluted to 5 mg/mL and the dispersion medium was deionized water. A scanning infrared spectrometer (Bruker, Karlsruhe, Germany) was used to scan at points between 400 cm^{-1} and 4000 cm^{-1}. Data between 1600 cm^{-1} and 1700 cm^{-1} were extracted for Gaussian fitting using OMNIC software and Peakfit 4.12 software, and the percentage contents of α-helix, β-sheet, β-turn, and random coil were calculated (Zhao et al., 2021).

2.4.4. Tryptophan fluorescence

MPs were diluted to 0.5 mg/mL using PBS (pH 6.0) and scanned for spectral information from 300 nm to 400 nm using a fluorescence spectrophotometer (F97 Shanghai Lengguang Technology Co., Ltd., Shanghai, China) with the excitation wavelength set at 295 nm (Pan, Ma, Diao, Li, & Chen, 2023).

2.4.5. Surface hydrophobicity

The concentration of MPs was adjusted to 5 mg/mL using PBS (pH 6.0), and 1 mL of MPs solution was pipetted into 200 μL of 1 mg/mL bromophenol blue (BPB), mixed well, and then the reaction mixture was shaken for 15 min. After the reaction was completed, the supernatant

was centrifuged at 5500 ×*g* for 15 min (4 °C), and the supernatant was taken and diluted 10-fold with PBS, and the absorbance value was measured at 595 nm (Model T6, General Instrument Co., Ltd., Beijing, China). PBS without MPs was used as a blank control (Pan et al., 2023). Surface hydrophobicity of MPs was expressed as the amount of BPB bound by MPs and was calculated as follows:

$$\text{MPs Surface hydrophobicity } (\mu g) = 200\ \mu g \times \frac{\mathbf{A_{control}} - \mathbf{A_{sample}}}{\mathbf{A_{sample}}}.$$

2.4.6. Ionic bonds and hydrogen bonds

The concentration of MPs was adjusted to 2 mg/mL using deionized water. Then 2 mL of MPs solution was added to 10 mL of 0.05 M sodium chloride (SA), 0.6 M sodium chloride (SB), and 0.6 M SB mixed with 1.5 M urea (SC), respectively, and incubated at 4 °C away from light for 1 h, and centrifuged at 12,000 ×*g*, 4 °C for 15 min. The protein content in the supernatant was determined by a BCA kit, and ionic bonds were expressed as the difference between the protein content in the SB solution and the SA solution, and hydrogen bonds were expressed as the difference between the protein content in the SC solution and the SB solution in mg/mL (Qian et al., 2019).

2.5. Redox proteomic analysis

2.5.1. Protein extraction and biotin labeling

MPs samples (200 μg) were ground in liquid nitrogen and 500 μL of SDT buffer was added, the mixture was then sonicated in an ice-water bath for 2 min, and centrifuged at 14,000 ×*g*, at 4 °C for 15 min, and the supernatant was taken. Protein quantification was performed using the BCA method. NEM (adjusted to a final concentration of 20 mM) was added to each MPs sample, and the mixture was incubated at 60 °C for 30 min. NEM was removed using the trichloroacetic acid-acetone precipitation method, and the protein precipitate was re-dissolved in PBS (pH 7.4) containing 4 % SDS, 5 mM of TCEP, and the protein precipitates were incubated at 50 °C for 1 h to reduce oxidation sites. TCEP was further removed using TCA-acetone precipitation. The treated MPs samples were redissolved in 1 mL of PBS (pH 7.4) buffer (containing 4 % SDS), and then 1 mL of PBS, 3 mL of ultrapure water, protease inhibitor, 5 mM EDTA, and 500 μL of 4 mM Biotin-HPDP (containing DMSO) were added, mixed, and then incubated at 25 °C for 3 h. The proteins were concentrated by 5 kDa ultrafiltration tubes, followed by precipitation using cold acetone in the dark overnight. The protein precipitates were sonicated on ice, mixed, and trypsinized for 12 h. After digestion, the peptides were desalted using a C18 Cartridge (Maisch, Ammerbuch Entringen, Germany) and lyophilized by vacuum concentration.

2.5.2. Oxidized peptide enrichment

Briefly, 1 mg of MPs peptide was added with Loading buffer to fully dissolve, then 100 μL of high binding capacity Chain Affinity Agarose Resin was added, and incubated at room temperature for 3 h. Then 1 mL of Loading buffer was added and the resin particles were washed with PBS for 4 times. Peptides were eluted by adding 100 μL Elution buffer (50 mM NH_4HCO_3, pH 8.2) and 5 mM TCEP. The above operation was repeated once, the eluates were combined, IAA was added to adjust the concentration to 20 mM, and then incubated at room temperature away from light for 1 h. The peptides were desalted by C18 Cartridge and freeze-dried to obtain the oxidized peptides.

2.5.3. LC-MS/MS

Peptides were separated by chromatography using a nanoliter flow rate chromatography system (Easy-nLC1200 Thermo Scientific, Massachusetts, USA). The buffers were set as solution A (0.1 % formic acid solution) and solution B (0.1 % formic acid, 95 % acetonitrile and water mixture, *v:v:v*, 1:1:1). The samples were injected into a C18 trap column and then passed through a C18 chromatographic analytical column for gradient separation, and the flow rate was set at 300 μL/min. The gradient of liquid chromatographic separation was as follows: 0–2 min, the linear increase of liquid B was 2 % to 5 %; 2–99 min, the linear increase of liquid B was 5 % to 28 %; 99–111 min, the linear increase of liquid B was 28 % to 40 %; 111–113 min, the linear increase of liquid B was 40 % to 100 %; and 113–120 min, the linear increase of liquid B was maintained at 100 %. The peptides were separated and analyzed by DDA (data dependent acquisition) mass spectrometry using a mass spectrometer. The length of analysis was 120 min. Detection mode: positive ion, parent ion. Scanning range: 350–1800 *m/z*, primary mass resolution: 60000 @m/z 200, AGC target: 3e6, primary Maximum IT: 50 ms. Peptide secondary mass spectra were acquired according to the following method: each full scan triggered the acquisition of secondary mass spectra (MS2) of the 20 highest intensity parent ions. scan), secondary MS resolution: 15,000 @ m/z 200, AGC target: 1e5, secondary Maximum IT: 50 ms, MS2 Activation Type: HCD, Isolation window: 1.6 m/z, Normalized collision energy: 28.

2.5.4. Database searching

Mass spectrometry data were retrieved utilizing the mass spectrometry database search software, Proteome Discoverer 2.4. The protein database was the Uniprot-*Bos taurus* (Bovine) [9913]-47,135–0613.fasta, comprising a total of 47,135 protein sequences, which was downloaded on June 13, 2022. Database schema set to target-antipode, peptide spectra matched to (PSM match), FDR set to 0.01, Protein Quantification Razor and unique peptides were used for protein quantification.

2.6. Molecular simulation docking

Molecular docking of ·OH and MPs was performed using Python (PSF, New York, USA) and AutoDock vina (Version 2.0.5 The Scripps Research Institute, California, USA) to determine the mode of oxidation between ·OH and MPs macromolecules. The ·OH search Pubchem (https://pubchem.ncbi.nlm.nih.gov/) for Compound CID (CID_157350). Molecular structures in PDB format were sourced from Uniport database (https://www.uniprot.org/) and PDB database (https://www.rcsb.org) annotated proteomics data. Docking was simulated using Chem 3D to convert the 2D ·OH into a 3D structure. Prior to docking, proteins and small molecule compounds in MPs and ·OH PDB formats were dehydrogenated and hydrogenated using AutoDock and converted to PDBQT, with reference to Table 1 oxidation site setting BOX format 20 × 20 × 20, semi-flexible docking was used, and other parameters were set to the default values. Then 100 docking runs were performed based on the Lamarck algorithm, the docking results were output in DLF format, and the docking results including bond energies, amino acid sites, etc., were viewed and the docking diagram in PDBQT format exported. The PDBQT format results were converted to PDB using Open Babel, and the docking results in PDB format were viewed using the researcher's home (https://www.home-for-researchers.com/static/index.html#/).

2.7. Statistical analysis

Results were expressed as mean ± standard deviation (SD). Significance was analyzed using the LSD test for one-way ANOVA using SPSS 25 software (SPSS Inc., Chicago, IL, USA) and the significance threshold for statistical analysis was set at $p < 0.05$. Graphs were plotted using Origin 2021 software (OriginLab, Northampton, MA, USA).

3. Results

3.1. Effect of ·OH oxidation of MPs on their quality characteristics

The MFI and moisture distribution of MPs were analyzed in order to assess the potential effects of ·OH oxidation on the structure of MPs as well as on meat quality. The MFI increased significantly ($p < 0.05$) with the enhancement of the degree of oxidation (0–20 mM) (**Fig. 1**a),

Table 1
Fenton oxidation system induced MP oxidation sites identified by cysteine oxidation protein modification histology.

No.	Uniport ID	Annotated Sequence	Positions in Master Proteins	Protein Name	Log10 (Control)	Log10 (Fenton)	Fold Change	*P.* value
1	A0A3Q1MZN6-(C71)	[R].QGEYICTQDYQR.[L]	[66–77]	Actin binding LIM protein family member 2	7.031 ± 0.033	6.633 ± 0.057	2.49	0.0008
2	A0A3Q1MZN6-(C177)	[K].HWHLGCFK.[C]	[172–179]	Actin binding LIM protein family member 2	6.947 ± 0.060	5.876 ± 0.047	11.80	0.0008
3	A0A3Q1LWM1-(C91)	[R].VVVIESVLCPSHFR.[E]	[83–96]	Actin-related protein 10	6.449 ± 0.018	3.687 ± 0.000	578.22	0.0000
4	A0A3Q1M6W4-(C179)	[RK].AIMTYVSCFYHAFAGAEQAETAANR.[I]	[172–196]	Alpha-actinin-2	7.549 ± 0.014	6.214 ± 0.275	17.92	0.0000
5	Q0III9-(C593)	[K].ICQTYGLRPSSTNPYITLTPQDINTK.[W]	[592–617]	Alpha-actinin-3	8.470 ± 0.035	7.877 ± 0.021	3.93	0.0002
6	Q5E9B5-(C258)	[R].FRCPETLFQPSFIGMESAGIHETTYNSIMK.[C]	[256–285]	Actin, gamma-enteric smooth muscle	6.907 ± 0.054	5.125 ± 1.017	17.35	0.0005
7	P60712-(C272)	[R].CPEALFQPSFLGMESCGIHETTFNSIMK.[C]	[257–284]	Actin, cytoplasmic 1	6.459 ± 0.055	5.811 ± 0.176	4.12	0.0029
8	Q27966-(C498)	[K].GIISILDEECLRPGEATDLTFLEK.[L]	[489–512]	Unconventional myosin-Ic	6.237 ± 0.059	3.687 ± 0.000	358.17	0.0005
9	Q5E997-(C157)	[K].KIDGQQTIIACIESHQFQAK.[N]	[147–166]	F-actin-capping protein subunit alpha-2	7.652 ± 0.048	7.222 ± 0.062	2.68	0.0020
10	A6QR13-(C213)	[K].ACEVFEAQECER.[I]	[212−223]	PSTPIP2 protein	5.905 ± 0.054	3.687 ± 0.000	166.31	0.0003
11	A6QR13-(C221)	[K].ACEVFEAQECER.[I]	[212–223]	PSTPIP2 protein	5.905 ± 0.054	3.687 ± 0.000	166.31	0.0003
12	A0A3Q1LV98-(C439)	[R].CTYRPVMEGPHTVHVAFAGAPITR.[S]	[439–462]	Filamin C	6.640 ± 0.073	3.687 ± 0.000	911.04	0.0013
13	A0A3Q1LV98-(C1654)	[K].CLVTVSIGGHGLGACLGPR.[I]	[1640–1658]	Filamin C	7.794 ± 0.041	7.470 ± 0.014	2.12	0.0014
14	A0A3Q1LV98-(C645)	[R].YWPTEPGEYAVHVICDDEDIR.[D]	[631–651]	Filamin C	7.627 ± 0.039	7.248 ± 0.023	2.40	0.0008
15	A0A3Q1LV98-(C1406)	[K].DGSCTVEYIPFTPGDYDVNITFGGRPIPGSPFR.[V]	[1403–1435]	Filamin C	6.735 ± 0.029	3.687 ± 0.000	1119.07	0.0000
16	Q3ZBU0-(C104)	[K].LEPVPVQKPTVTSVCAETAQELAEGQR.[R]	[90–116]	PDZ and LIM domain 5	7.858 ± 0.023	7.407 ± 0.046	2.81	0.0001
17	A4IFK4-(C286)	[R].VEVIFDCSDR.[Q]	[280–289]	SYNPO2 protein	6.941 ± 0.021	3.687 ± 0.000	1796.85	0.0000
18	F1MT60-(C667)	[K].DSYVQNVLGHYIGSFEDPYQVHCLK.[I]	[645–669]	Nebulin	7.155 ± 0.056	4.517 ± 1.173	28.61	0.0006
19	F1MT60-(C420)	[K].DILGHYVGSYEDPYHTHCMR.[VK]	[403–422]	Nebulin	8.015 ± 0.039	7.522 ± 0.035	3.11	0.0005
20	F1MT60-(C5040)	[R].LHLHEWICHPDLQVNSHVR.[K]	[5033–5051]	Nebulin	7.597 ± 0.068	3.687 ± 0.000	8224.98	0.0007
21	Q9BE40-(C816)	[R].RESIFCIQYNVR.[A]	[811–822]	Myosin-1	8.100 ± 0.054	7.300 ± 0.096	6.20	0.0007
22	E1BF23-(C678)	[K].HEEDLLGYYVDCSVAGSNVWEPCNHKPIGYNR.[F]	[667–698]	Myomesin 2	6.311 ± 0.234	4.335 ± 0.916	16.01	0.0460
23	E1BF23-(C1396)	[K].TLNLTCTVFGNPDPEVVWFK.[N]	[1391–1410]	Myomesin 2	7.277 ± 0.112	4.669 ± 1.388	13.66	0.0076
24	E1BF23-(C752)	[K].VQAALTVPSHPYGITLLNCDGHSMILGWK.[V]	[734–762]	Myomesin 2	6.405 ± 0.054	3.687 ± 0.000	526.23	0.0004
25	E1BF23-(C204)	[K].LCFTVQGFPTPVVQWYK.[D]	[203–219]	Myomesin 2	6.856 ± 0.079	6.203 ± 0.034	4.56	0.0046
26	E1BF23-(C470)	[K].ICKYPVTGLFEGR.[S]	[469–481]	Myomesin 2	6.293 ± 0.018	5.844 ± 0.116	2.71	0.0014
27	E1BCU2-(C1338)	[K].TLCLTCVVSGDPAPEIYWLK.[N]	[1336–1355]	Myomesin 3	5.974 ± 0.018	4.381 ± 0.982	4.73	0.0194
28	E1BCU2-(C1341)	[K].TLCLTCVVSGDPAPEIYWLK.[N]	[1336–1355]	Myomesin 3	5.974 ± 0.018	4.381 ± 0.982	4.73	0.0194
29	E1BCU2-(C761)	[K].ILGYFLDQHDSEELDWHEVNQQPVPTQICK.[V]	[733–762]	Myomesin 3	6.335 ± 0.154	3.687 ± 0.000	470.94	0.0105
30	E1BA80-(C1414)	[R].FKGDVACQVLESER.[A]	[1408–1421]	Myosin XVIIIB	6.337 ± 0.065	3.687 ± 0.000	451.84	0.0006
31	E1BA80-(C1481)	[R].FDCAQMENEFLR.[K]	[1479–1490]	Myosin XVIIIB	5.874 ± 0.015	4.954 ± 0.897	2.86	0.0218
32	Q3ZCL4-(C187)	[K].FHYLPFLPTTEDVYDCK.[V]	[172–188]	Major histocompatibility complex, class II, DR alpha	6.615 ± 0.080	6.140 ± 0.174	2.82	0.0128
33	A0A3Q1LWN6-(C823)	[R].NCAAYLK.[L]	[822–828]	Myosin heavy chain 11	6.745 ± 0.034	6.304 ± 0.055	2.74	0.0006
34	F1N0L9-(C304)	[R].WYCEGK.[E]	[302–307]	Myopalladin	6.177 ± 0.054	3.687 ± 0.000	311.01	0.0003

(*continued on next page*)

Table 1 (*continued*)

No.	Uniport ID	Annotated Sequence	Positions in Master Proteins	Protein Name	Log10 (Control)	Log10 (Fenton)	Fold Change	*P.* value
35	A6QP89-(C210)	[K].DKFDSCSFDLEVLESTGTTPNIDIR.[S]	[205–229]	MYBPC1 protein	7.765 ± 0.025	7.350 ± 0.016	2.61	0.0001
36	A6QPA6-(C814)	[R].RESIFCIQYNIR.[A]	[809–820]	MYH3 protein	8.002 ± 0.057	7.239 ± 0.050	5.80	0.0010
37	Q28086-(C21)	[R].SSVFLSWGKPIYDGGCEIQGYIVEK.[C]	[6–30]	Connectin (Fragment)	6.401 ± 0.047	3.687 ± 0.000	520.80	0.0002
38	A0A3Q1M1X4-(C268)	[R].CVCQEGFAGEDCR.[E]	[268–280]	Tenascin C	6.084 ± 0.029	3.687 ± 0.000	250.13	0.0000
39	A0A3Q1M1X4-(C270)	[R].CVCQEGFAGEDCR.[E]	[268–280]	Tenascin C	6.084 ± 0.029	3.687 ± 0.000	250.13	0.0000
40	A0A3Q1M1X4-(C279)	[R].CVCQEGFAGEDCR.[E]	[268–280]	Tenascin C	6.084 ± 0.029	3.687 ± 0.000	250.13	0.0000
41	A0A3Q1M1X4-(C377)	[R].CPSDCHER.[G]	[377–384]	Tenascin C	4.925 ± 0.049	4.589 ± 0.017	2.18	0.0024
42	A0A3Q1M1X4-(C381)	[R].CPSDCHER.[G]	[377–384]	Tenascin C	4.925 ± 0.049	4.589 ± 0.017	2.18	0.0024
43	O18977-(C263)	[R].CVCNPGYSGEDCGVR.[S]	[263–277]	Tenascin-X	6.762 ± 0.037	6.439 ± 0.050	2.10	00018
44	O18977-(C265)	[R].CVCNPGYSGEDCGVR.[S]	[263–277]	Tenascin-X	6.762 ± 0.037	6.439 ± 0.050	2.10	0.0018
45	O18977-(C274)	[R].CVCNPGYSGEDCGVR.[S]	[263–277]	Tenascin-X	6.762 ± 0.037	6.439 ± 0.050	2.10	0.0018
46	O18977-(C3921)	[R].DCGEEMQNGVSTSR.[T]	[3920–3933]	Tenascin-X	6.097 ± 0.008	3.687 ± 0.000	256.99	0.0000
47	O18977-(C341)	[R].TCPWDCGEGGR.[C]	[340–350]	Tenascin-X	5.943 ± 0.083	3.687 ± 0.000	183.75	0.0021
48	O18977-(C345)	[R].TCPWDCGEGGR.[C]	[340–350]	Tenascin-X	5.943 ± 0.083	3.687 ± 0.000	183.75	0.0021
49	P63315-(C35)	[K].AAFDIFVLGAEDGCISTK.[E]	[22–39]	Troponin C, slow skeletal and cardiac muscles	8.149 ± 0.026	7.800 ± 0.048	2.23	0.0005
50	Q4U0T9-(C58)	[K].ALDSTTVAAHESEIYCKVCYGR.[R]	[43–64]	Cysteine and glycine-rich protein 3	6.264 ± 0.193	4.411 ± 1.023	8.22	0.0364
51	Q4U0T9-(C61)	[K].ALDSTTVAAHESEIYCKVCYGR.[R]	[43–64]	Cysteine and glycine-rich protein 3	6.264 ± 0.193	4.411 ± 1.023	8.22	0.0364
52	Q2KI95-(C132)	[R].CQQPIGTK.[S]	[132–139]	Four and a half LIM domains protein 2	6.175 ± 0.039	5.803 ± 0.034	2.36	0.0010
53	Q2KI95-(C7)	[R].FDCHHCEDSLFGR.[K]	[5–17]	Four and a half LIM domains protein 2	6.629 ± 0.021	4.371 ± 0.967	22.96	0.0001
54	Q2KI95-(C10)	[R].FDCHHCEDSLFGR.[K]	[5–17]	Four and a half LIM domains protein 2	6.629 ± 0.021	4.371 ± 0.967	22.96	0.0001
55	Q3ZBI6-(C209)	[R].EDDPYCVTCFGELFAPK.[C]	[204–220]	Four and a half LIM domains protein 3	7.986 ± 0.034	7.673 ± 0.034	2.05	0.0011
56	Q3ZBI6-(C212)	[R].EDDPYCVTCFGELFAPK.[C]	[204–220]	Four and a half LIM domains protein 3	7.986 ± 0.034	7.673 ± 0.034	2.05	0.0011
57	Q3ZBI6-(C251)	[R].HWHHSCFSCAR.[C]	[243–253]	Four and a half LIM domains protein 3	7.101 ± 0.129	3.687 ± 0.000	2714.74	0.0108
58	Q3ZBI6-(C65)	[R].HFHEGCFR.[C]	[60–67]	Four and a half LIM domains protein 3	8.883 ± 0.018	8.521 ± 0.023	2.30	0.0001
59	Q3ZBI6-(C248)	[R].HWHHSCFSCAR.[C]	[243–253]	Four and a half LIM domains protein 3	6.920 ± 0.067	5.266 ± 1.117	11.06	0.0012

indicating that ·OH oxidation had a significant promoting effect on the structural degradation of MPs. As illustrated in Fig. 1b, the centrifugal loss of MPs in the 0–20 mM oxidation range increased (8.59 % to 11.02 %) significantly ($p < 0.05$) with the increase of oxidation.

Low-field nuclear magnetic resonance (LF-NMR) was further used to characterize the water distribution state of MPs. The LF-NMR spectra showed three peaks with different relaxation times (Fig. 1c). T_2 showed three peaks, T_{21} (0.02–2.01 ms), T_{22} (6.14–28.49 ms) and T_{23} (57.23–351.12 ms). Among them, T_{23} was the major water group. Therefore, it was hypothesized that T_{21} and T_{22} denote strongly bound and weakly bound water, respectively, and T_{23} denotes immobilized water (not easily mobile water). As shown in Fig. 1c-e, with the enhancement of oxidation, the LF-NMR water distribution showed different states, including the proportion of different water groups and the relaxation time T_2, suggesting that the oxidation of MPs by hydroxyl radicals altered the intermolecular interactions between MPs and water. As shown in Fig. 1d, with the enhancement of ·OH oxidation, T_{21} increased and then decreased, while T_{22} decreased and then increased, and the overall percentage of T_{21} and T_{22} attended to decrease (from 2.54 % to 1.72 %). T_{23} tended to increase (from 97.46 % to 98.28 %). In addition, the peak area decreased with the enhancement of the ·OH oxidation (Fig. 1e).

3.2. *Effect of ·OH oxidation of MPs on their structural characteristics*

In this investigation, ·OH oxidation of MPs was generated using the Fenton oxidation system with carbonyl and sulfhydryl groups to characterize the oxidation state of MPs. As illustrated in Fig. 2 a and b, the carbonyl content of MPs increased significantly ($p < 0.05$) with enhanced ·OH oxidation from 0.329 ± 0.014 to 1.2117 ± 0.089 nmol/g proteins. The level of sulfhydryl groups decreased significantly (from 0.0361 ± 0.0024 to 0.0157 ± 0.0004 mmol/mg proteins, $p < 0.05$) with increasing H_2O_2 concentration. Carbonyl and sulfhydryl levels indicated that hydroxyl radical levels were positively correlated with MPs oxidation. Considering the effect of protein oxidation on their structures, the primary, secondary and tertiary structures, and intermolecular forces of

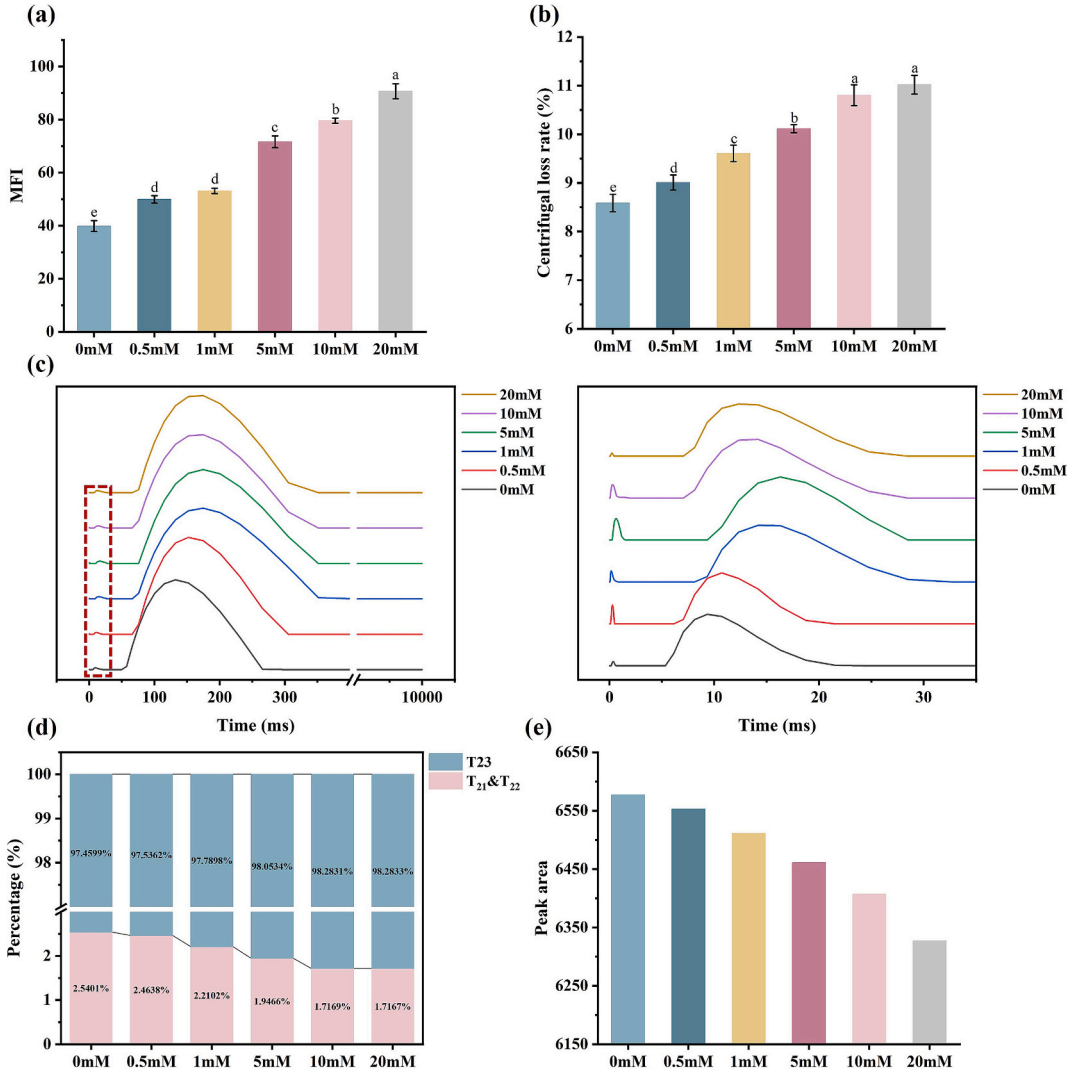

Fig. 1. (a) Effect of ·OH oxidation system on MFI of MPs. (b) Effect of ·OH oxidation system on centrifugal loss of MPs. (c) Transverse relaxation time T_2 inversion profile of hydrogen proton signal. (d) Percentage change in T_2 relaxation peak area. (e) Change in lateral relaxation time peak area. T_{21} indicates strongly bound water. T_{22} indicates weakly bound water. T_{23} indicates immobilized water (not easily mobile water). Significant differences are indicated between different letters (a-e) ($p < 0.05$).

MPs were further evaluated (Fig. 2c). The protein species did not differ despite the concentration gradient of H_2O_2 in the Fenton oxidation system. The electropherograms showed the molecular weight distribution of myosin heavy chain (MHC, 220 kDa), paramyosin (100 kDa), actin (43 kDa), tropomyosin and troponin-T (35 kDa), troponin-I (28 kDa) and myosin light chain (MLC, 16–25 kDa), and a clear band presumed to be myosin (480 kDa) was observed in the upper part of the MHC. Actin and MHC were the most abundant MPs bands observed, and none of the bands showed significant degradation or cross-linking.

As shown in Fig. 2d and e, the spectral scanning range had obvious absorption peaks in the interval of 1600–1700 cm^{-1}. The amide bands were analyzed for the secondary structure of the MPs protein, and the secondary structure was calculated as the proportion of α-helix, β-sheet, β-turn and random coil. With the increase of H_2O_2 level, protein secondary structure was mainly characterized by an increase in the proportion of random coil. For example, the random coil level increased from 26.18 % to 35.11 % at the concentration of 20 mM, while the β-turn and α-helix decreased by 10.69 % and 11.89 %, respectively (Fig. 2e). The exposure index of tryptophan reflects the tertiary structural changes of the protein, and the intensity of tryptophan's intrinsic fluorescence decreases progressively with the enhancement of ·OH oxidation (Fig. 2f). The protein secondary and tertiary structural changes indicate that ·OH oxidation promotes the unfolding of the protein structure. With the enhancement of ·OH oxidation system, the surface hydrophobicity increased ($p < 0.05$) (Fig. 2g), and the BPB binding of 20 mM-treated MPs grew from 37.52 ± 0.48 to 56.37 ± 1.32 μg, with a growth rate of 50.24 %. Compared to the control group at 0 mM, both ionic bonding and hydrogen bonding decreased significantly with the intensification of Fenton oxidation, dropping from 1.743 ± 0.008 mg/mL and 1.308 ± 0.009 mg/mL to 1.321 ± 0.04 mg/mL and 0.557 ± 0.023 mg/mL, respectively. This corresponds to reductions of 24.21 % and 57.42 % ($p < 0.05$) (Fig. 2h and i). These results suggest that the oxidative modification behavior of ·OH promotes MPs structural stretching and reduces intermolecular forces.

3.3. Cys redox modification proteomics

3.3.1. Quality control of redox-modified proteomics

Next, in order to screen and characterize the potential Cys oxidation sites of MPs oxidized by ·OH from the Fenton reaction, an in vitro Fenton reaction model of MPs was constructed. The MPs were analyzed by SDS-PAGE gel electrophoresis (1D). The protein bands were similar in different groups (Fig. 3a), indicating that the levels of proteins were similar. The effect of Fenton reaction on MPs oxidation was determined

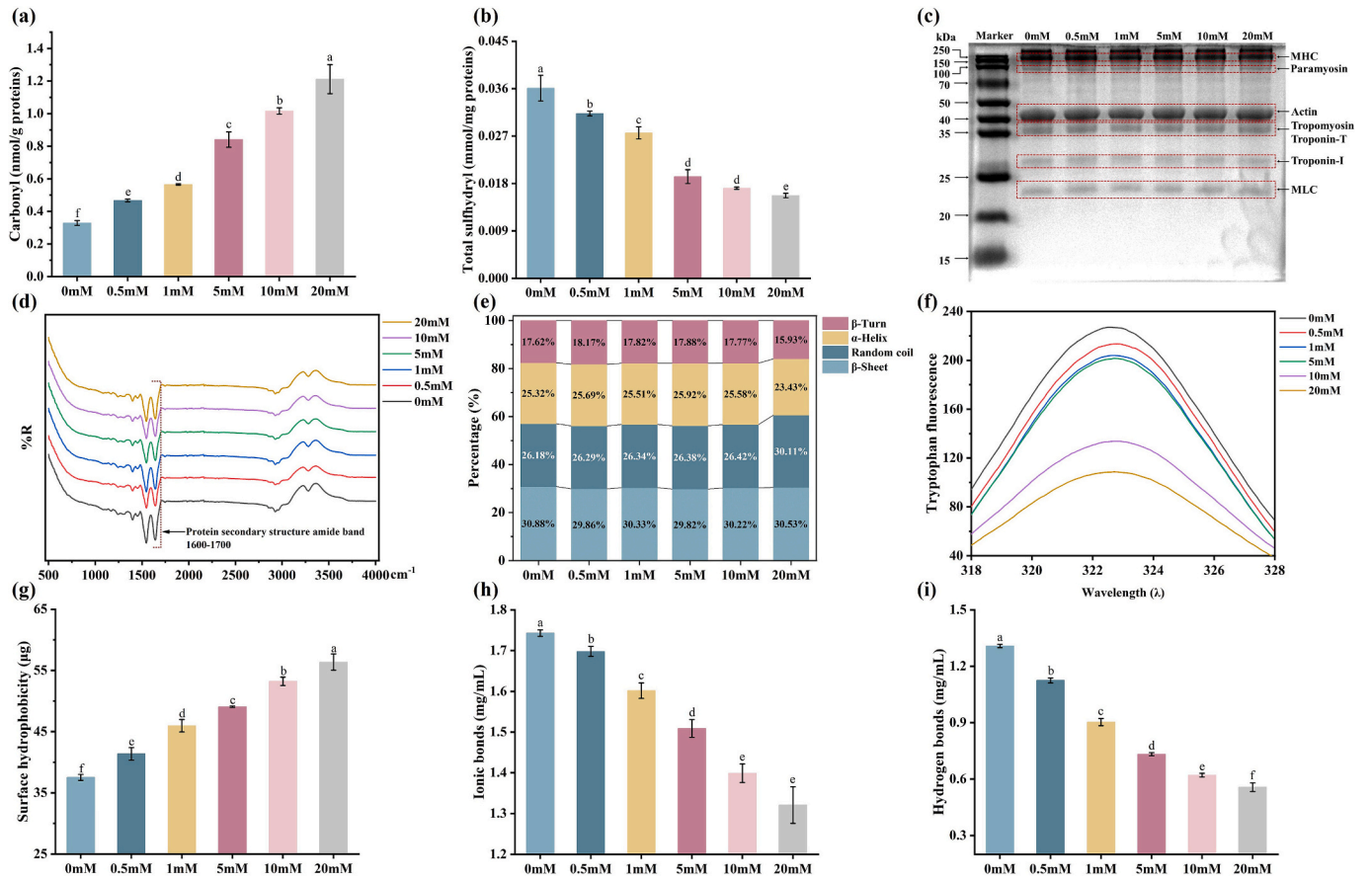

Fig. 2. (a) Effect of ·OH oxidation on carbonyl level of MPs. (b) Effect of ·OH oxidation on sulfhydryl level of MPs. (c) SDS-PAGE protein spectra of ·OH oxidation-treated MPs. (d) FT-NIR spectra spectra. (e) Effect of ·OH oxidation on the secondary structure of MPs. (f) Tryptophan fluorescence spectra of MPs treated with ·OH oxidation. (g) Effect of ·OH oxidation on the surface hydrophobicity of MPs. (h) Effect of ·OH oxidation on the ionic bonding level of MPs. (i) Effect of ·OH oxidation on hydrogen bonding level of MPs. Significant differences are indicated between different letters (a-e) ($p < 0.05$).

by assessing the intra-group similarity and inter-group variability of the two groups of MPs, as shown in Fig. 3b, the intra-group correlation coefficients were 0.97–0.98 for Control and 0.98–0.985 for Fenton group. The inter-group correlation coefficients between Control and Fenton groups were 0.929–0.934, and the inter-group similarity was much lower than the intra-group similarity, indicating that Fenton treated sample proteins had good inter-group variability and intra-group reproducibility, and Fenton treatment had a significant effect on MPs.

3.3.2. *Cys oxidation sites in MPs*

Differential modification sites between Control and Fenton samples were screened by fold change (FC) and one-way ANOVA, followed by *t*-test (*p* value). A total of 1192 differentially oxidized loci were identified using FC > 2 and $p < 0.05$ as screening criteria (Table S1). Significant differences between the two sample groups were shown using clustered heatmaps, with up-regulation (UP) in red and down-regulation (DOWN) in green, with 774 UP oxidation sites and 418 DOWN oxidation sites, and the clustered heatmaps showed intra-group similarities and inter-group differences, with higher similarity between data patterns of similar color within the groups, and lower similarity between the groups with significant differences in the color of the data patterns (Fig. 3c). GO functional annotation of proteins with modification sites between samples was performed. The main functions of proteins include biological process (BP), molecular function (MF), and cellular component (CC). In this study, although the proteins in the hydroxyl radical oxidation model were separated and purified, a considerable proportion of other proteins still exhibit highly sensitive cysteine modifications (**Fig. S1**). As the most abundant CC in bovine muscle tissue, MPs were further screened for Cys oxidation site proteins of CC. Fig. 3d displays the top 50 CC proteins (oxidative site proteins) annotated by GO function, in which MPs were mainly myofibril, contractile fiber, sarcomere, supramolecular fiber, myosin filament, actin cytoskeleton, cardiac myofibril and I-band, with the highest content being myofibrils. A total of 59 Cys oxidation sites of MPs were identified, including actin (17), myosin/myomesin (16), tenascin (12), sarcomere (10), nebulin (3) and troponin (1) (Table 1). Motif analysis of the modified site sequences confirmed a significant enrichment of redox-sensitive cysteines (C) at the +7 position. Additionally, tryptophan (W) residues were markedly enriched at the +11 position (Fig. 3E), indicating that the most conserved group in hydroxyl radical-induced redox modifications of cysteines is '-C-X-X-X-W-'. Specifically, Q0III9 (C593), E1BF23 (C204, C470, C678, C752, C1396), E1BCU2 (C761, C1341, C1338), and O18977 (C341) exemplify the amino acid sequence characteristics observed in Fig. 3E.

3.4. *Molecular simulation of docking for ·OH oxidation of MPs Cys*

The GO functionally annotated proteins with 59 Cys different sites were annotated to the UNIPORT and PDB databases to obtain the structural information of the proteins, and molecular simulation docking was performed by AutoDock. As shown in Table 2 and Fig. 4, a total of 12 ·OH and MPs protein binding sites and structures were identified. Notably, the 12 molecularly mimicked oxidation sites were consistent with the Cys oxidation sites identified by redox protein modification histology (Table 2). The results indicated that the sites identified by redox protein modification histology were reliable, and the Fenton oxidation system changed the MPs structure and intermolecular forces

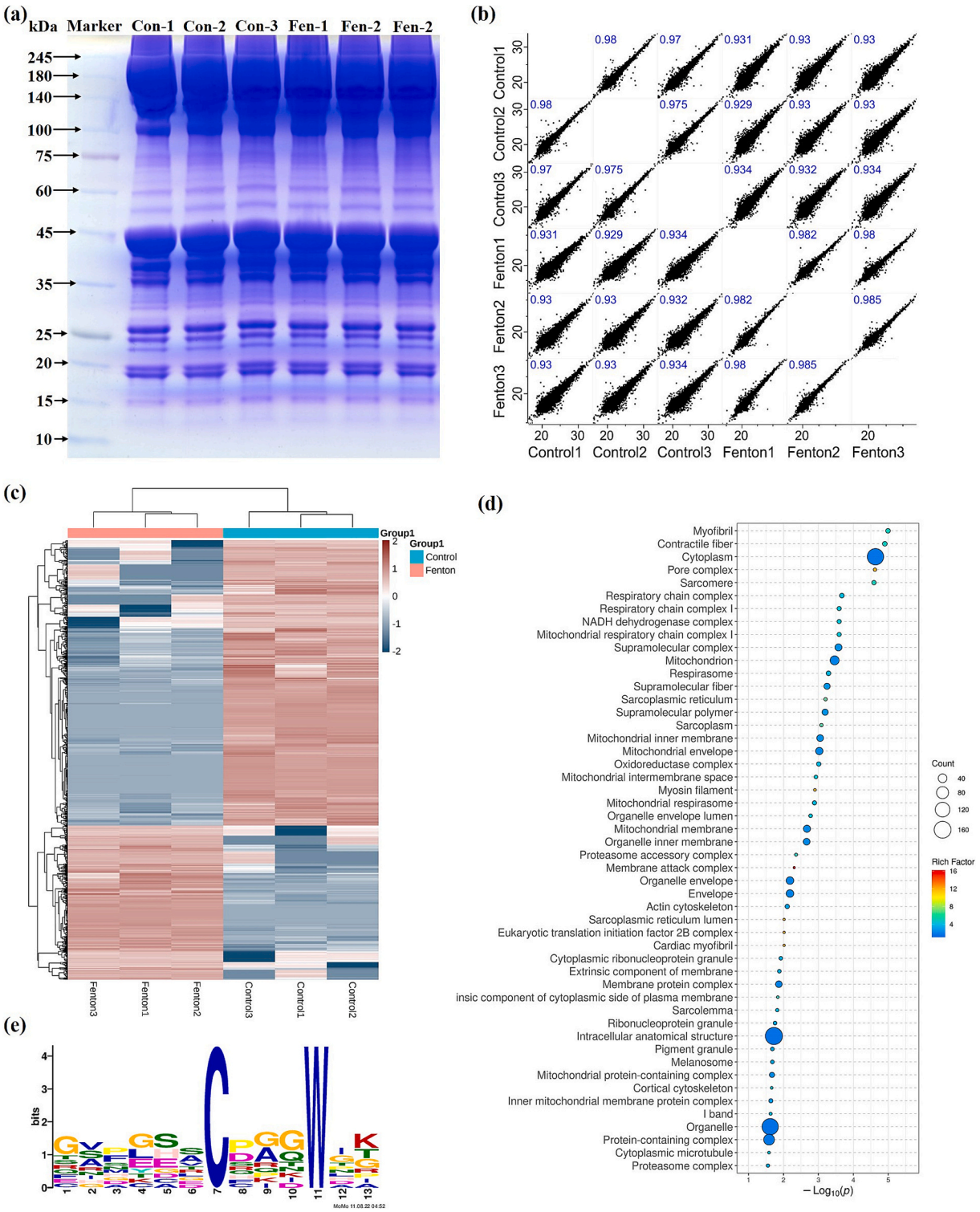

Fig. 3. (a) SDS-PAGE gel electrophoresis protein profile. (b) Distribution map of correlation coefficients of sample protein expression. (c) Clustering heat map of cysteine redox sites. (d) Proteins of the top 50 cellular component proteins for GO functional annotation. (e) Most conserved motifs of redox-modified cysteine.

by oxidizing Cys in the MPs protein structure.

4. Discussion

The unavoidable production of ·OH during post-slaughter muscle tissue aging is due to the Fenton reaction, and the most classical pathway for ·OH generation involves the conversion of Fe (II) to Fe (III) and ·OH by the reaction of Fe (II) with H_2O_2. Beef has higher levels of iron ions compared to other meats, providing ligands for ·OH generation which is a prerequisite for initiating the Fenton reaction (Liu et al., 2022). The ·OH generated by the Fenton reaction are characterized by high electrode potential, electrophilicity and diffusion-controlled rates, and undergo diffusive reactions with almost all biomolecules, which can result in a wide range of non-selective and site-specific attacks on biomolecules, and are considered to be powerful oxidizing species (Zhao, 2023). Especially in biological systems, ·OH causes oxidative damage to

Table 2
Molecular simulation docking of ·HO and MPs Cys oxidation binding sites.

No.	Uniport ID	Annotated Sequence	Positions in Master Proteins	Site	Protein Name	Molecular bond energy (kJ/mol)
1	A0A3Q1LWM1	[R].VVVIESVLCPSHFR.[E]	[83–96]	91	Actin-related protein 10	−1.07
2	A0A3Q1M6W4	[RK].AIMTYVSCFYHAFAGAEQAETAANR.[I]	[172–196]	179	Alpha-actinin-2	−0.76
3	Q5E9B5	[R].FRCPETLFQPSFIGMESAGIHETTYNSIMK.[C]	[256–285]	258	Actin, gamma-enteric smooth muscle	−1.47
4	P60712	[R].CPEALFQPSFLGMESCGIHETTFNSIMK.[C]	[257–284]	272	Actin, cytoplasmic 1	−0.34
5	Q27966	[K].GIISILDEECLRPGEATDLTFLEK.[L]	[489–512]	498	Unconventional myosin-Ic	−0.87
6	A6QR13	[K].ACEVFEAQECER.[I]	[212–223]	221	PSTPIP2 protein	−8.72
7	A4IFK4	[R].VEVIFDCSDR.[Q]	[280–289]	286	SYNPO2 protein	−1.1
8	Q9BE40	[R].RESIFCIQYNVR.[A]	[811–822]	816	Myosin-1	−0.76
9	Q3ZBI6	[R].EDDPYCVTCFGELFAPK.[C]	[204–220]	209	Four and a half LIM domains protein 3	−0.65
10	Q3ZBI6	[R].EDDPYCVTCFGELFAPK.[C]	[204–220]	212	Four and a half LIM domains protein 3	−0.04
11	Q3ZBI6	[R].HWHHSCFSCAR.[C]	[243–253]	251	Four and a half LIM domains protein 3	−1.72
12	Q3ZBI6	[R].HWHHSCFSCAR.[C]	[243–253]	248	Four and a half LIM domains protein 3	−1.27

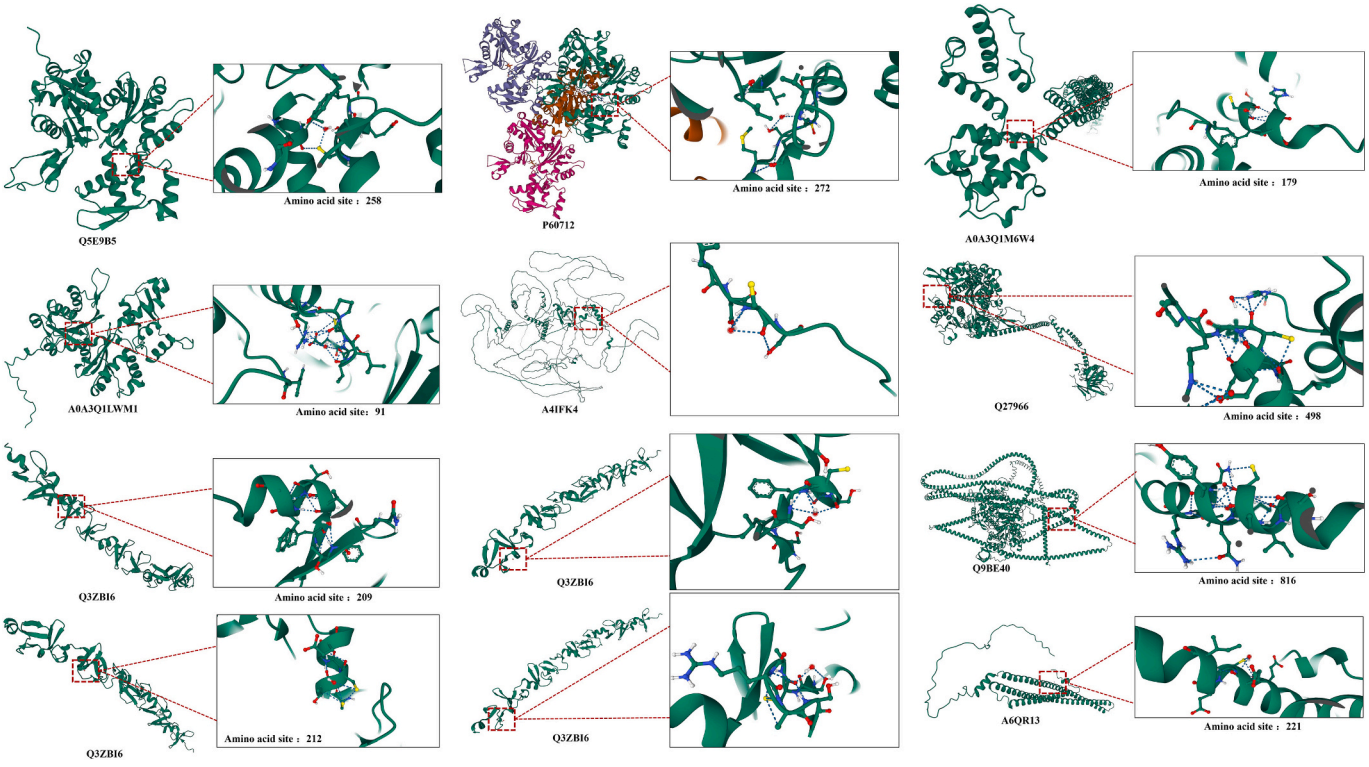

Fig. 4. Schematic diagram of the molecularly simulated docking structure of the ·OH and MPs Cys oxidation binding site.

DNA, lipids, proteins and cells, inducing oxidative stress. This is consistent with the result of the present study that ·OH significantly induced oxidation of MPs (**Fig. 2**a and b). To be precise, oxidation by ·OH is a protein modification process, e.g., carbonylation is essentially a ·OH-mediated oxidative deamination of basic amino acids (lysine, threonine, arginine, and proline), in which ·OH attacks the ε-amino group in basic amino acids by seizing hydrogen atoms from adjacent carbon atoms of the amino acid chain, leading to the formation of iminos in the first step, an intermediate which is extremely unstable to undergo hydrolysis to form the corresponding protein carbonyl group (Estevez, Diaz-Velasco, & Martinez, 2022). In addition, the sulphur atoms of sulphur-containing amino acids in proteins, such as Cys, are highly reactive to oxidation, and Cys is converted to disulphide bonds and Cys oxyaicds (sulfenic acids, sulfonic acids and sulfinic acids), which results in the reactive sulfhydryl group being oxidized to form a disulphide bond, leading to a decrease in the content of reactive sulfhydryl groups (Zhang, Li, Hong, & Luo, 2021). Therefore, in this study, protein oxidation was assessed by the carbonyl and sulfhydryl levels of proteins (**Fig. 2**a and b), while confirming that the oxidation of myofibrillar proteins by ·OH was a process of amino acid modification.

The·OH-mediated oxidation of Cys in a protein is thought to be the primary mechanism of redox signalling, with the sulfhydryl groups of Cys being deprotonated to form reversible or irreversible redox-dependent post-translational modifications (PTM) (Duan, Gaffrey, & Qian, 2017). The molecular simulation docking results verified that ·OH bound efficiently to Cys via hydrogen bonding (Fig. 4 and Table 2) with redox modifications. It is important to emphasise that the Cys proteome contains 214,000 Cys with thiol structures or other forms that vary in

their PTM signatures, with reversible Cys redox PTM considered to be the primary redox signalling and regulation, whereas the irreversible modifications of sulfenylation (SO_2H) and sulphonylation (SO3H), reflecting over-oxidation, are considered to be markers of oxidative stress (Jones & Go, 2011). Given the complexity of Cys redox modifications, a reaction system for hydroxyl radicals and myofibrillar proteins was constructed in this study. As illustrated in **Fig. 3**E, the amino acid sequences enriched at cysteine oxidation sites exhibit a distinctive motif characterized by the -C-X-X-X-W- sequence structure. Notably, the oxidative modifications of cysteine are influenced by the presence of adjacent tryptophan residues. Jiao et al. (2021) have proposed that cysteine-related modifications may also be impacted by the steric hindrance of other neighboring amino acids, which aligns with the findings of this study. The inactivation of the antioxidant system is due to the transformation of the metabolic activity of the slaughtered muscle, which inevitably leads to a reversible Cys redox to an irreversible shift, determined by oxidative stress. The formation of redox PTM in organisms is relatively complex and involves biological processes mainly mediated by enzymatic reactions or reactions mediated by oxidatively active substances (ROS/RNS/RSS) (Behring et al., 2014). For Cys residues, their oxidative sensitivity is mainly related to solvent accessibility, thiol pKa, subcellular localisation and microenvironmental status. It has been reported that specific Cys residues in all subcellular compartments and functional proteins can be oxidized, including cytoskeletal proteins, such as actin, myosin and microtubule proteins (Jones & Go, 2011). In the study, 59 Cys oxidative modification sites were identified, mainly actin (17), myosin/myomesin (16), tenascin (12) and sarcomere (10) (Table 1). Actin (43 kDa) was overwhelmingly dominant in the MPs system (**Fig. 2**c), with the most Cys sites modified by ·OH redox.

The Cys oxidation is characterized by the oxidation of sulfhydryl groups to generate disulphides, and this cross-linking of disulphides causes changes in protein structure, either by degradation or formation of protein aggregates (Bao & Ertbjerg, 2019). It was expectedly found that even at the highest oxidized concentration (20 mM) MPs did not show significant degradation or formation of protein aggregates (**Fig. 2**c). Decker, Xiong, Calvert, Crum, and Blanchard (1993) reported that oxidation of MPs would lead to cross-linking of myosin and actin to form larger molecular weight aggregates. Notably, MFI showed enhanced protein fragmentation or degradation with increased oxidation (**Fig. 1**a). It is generally accepted that intermolecular hydrophobic interactions and intermolecular covalent bonds, such as S—S bridges, facilitate protein aggregation (Li, Xiong, Subramanian, Suman, & True, 2024). Both cysteine and tryptophan are acidic amino acids that can serve as proton donors to hydroxyl radicals, thereby displaying a heightened sensitivity to oxidation (Li et al., 2024), which is consistent with the results of the present study, as shown in **Fig. 3**E, which demonstrates that redox modification histology identifies Cys and Tryptophan as highly sensitive. That's why oxidative modifications tend to cluster around cysteine and tryptophan residues (**Fig. 3**E). The disulfide bonds formed by cysteine are particularly critical for maintaining tertiary structure stability. Notably, the topology of disulfide bonds is fundamental to the analysis of primary structure homology, with cysteine residues being highly conserved among homologous proteins. In contrast, tryptophan is statistically more conserved than cysteine (Gilbert, 2013). This suggests that the oxidative modification of cysteine and tryptophan disrupts the formation of disulfide bonds. The results of protein secondary and tertiary structure and intermolecular forces showed (Fig. 2) that the increase in the proportion of irregular curls was characteristic of protein structural stretching, the decrease in tryptophan fluorescence may be due to the oxidative degradation of tryptophan and its conversion to free radicals, this is consistent with the sequence results presented in **Fig. 3**E. The hydrophobicity of proteins is important for the folding of the secondary structure inside them or the formation of structural domains of proteins, tertiary structure, etc., through hydrophobic interactions (Estévez, Kylli, Puolanne, Kivikari, & Heinonen, 2008; Jia, Wang, Shao, Liu, & Kong, 2017). Therefore, it is speculated that the irreversible oxidative modification of Cys focuses more on protein degradation not formation of protein aggregates. Gao et al. (2024) reported that oxidative stress increased MFI index through induced protein structural damage, consistent with our findings.

Cys redox-mediated changes in the structure and spatial pin arrangement of MPs are key factors influencing muscle texture and water holding capacity. Protein oxidation is negatively correlated with tenderness, a view based on the fact that protein oxidation promotes cross-linking of MPs through inhibiting hydrolysis of MPs by calpain (Malheiros et al., 2019). Another view is that oxidative degradation of MPs has an ameliorating effect on muscle tenderness. In the study, the MFI index increased, indicating that I-band and myofibrillar interconnections break. The results validate that Cys redox is a potential factor in the improvement of muscle tenderness through the degradation of MPs (Zhang et al., 2020). The effect of this oxidation on water retention, on the other hand, was negative (Fig. 1b-e), with a tendency to decrease both water binding and content. T_{21} and T_{22} are water molecules that are tightly bound to hydrophilic groups within the MPs by electrostatic forces, and this part of the water is stable and almost unaffected by physical stress. As oxidation enhances the intermolecular forces within the MPs itself, including hydrophobicity interactions, alteration of ionic bonds, and hydrogen bonds, this leads to a decrease in the binding of water to the MPs and the conversion of the bound water to free water or fixed water (Liu et al., 2022). Protein degradation also leads to a decrease in water retention as muscle cell contraction squeezes intracellular water into the extracellular space (Bao & Ertbjerg, 2019; Li et al., 2023). Overall, the effects of Cys redox modification of MPs on meat quality need to be viewed in a dialectical manner.

5. Conclusions

Redox proteomics and molecular modelling applied to probe specific patterns of oxidative modification of amino acids is feasible. The extensive oxidative modification of Cys by ·OH was attributed to 1192 differential oxidation sites (Dos) identified by redox proteomics, which contained a large number of Cys oxidation sites that were not in other proteins. Notably, 59 Dos were identified for myofibrillar proteins, of which actin (Cys 91, 179, 1406, 286), and myosin (Cys 268, 270, 279, 3921) and the amino acid sequence of the -C-X-X-X-W- structure were highly sensitive. MPs sulfhydryl groups, carbonyl groups, intermolecular forces, and structural information, on the other hand, confirmed that oxidative modification of Cys promoted the degradation of MPs structure. The study may provide an idea that masking or exposing Cys may can directionally modulate the meat aging procedure for meat quality maintenance and enhancement.

Funding

This study was financially supported by the Hubei Normal University 2023 Talent Introduction Project (HS2023RC084), Supportedby Hubei Provincial Natural Science Foundation of China (2024AFB162), Hubei Key Laboratory of Edible Wild Plants Conservation and Utilization Open Fund (EWPL202304), Hubei Provincial Department of Education's Science Research Program for Young Talents (Q20232506), and Centralized Local Science and Technology Development Funds (Laboratory Major Scientific and Technological Achievement Transformation) Project (2024BSB020).

CRediT authorship contribution statement

Jiale Li: Writing – review & editing, Writing – original draft, Software, Methodology, Data curation. **Jun Liu:** Writing – review & editing, Writing – original draft, Visualization, Supervision, Project administration, Investigation, Funding acquisition, Formal analysis, Data curation, Conceptualization. **Hui Yue:** Methodology, Data curation. **Yuanyuan Ma:** Investigation. **He Li:** Investigation. **Yuanliang Hu:** Supervision,

Project administration. **Xiang Yu:** Project administration. **Weiwei Dong:** Resources, Project administration. **Yanli Feng:** Resources, Project administration.

Declaration of competing interest

The authors declare that they have no known competing financial interests or personal relationships that could have appeared to influence the work reported in this paper.

Acknowledgments

We thank Gaolong Yin at Shanghai Bioprofile Technology Company Ltd. for his technical support in proteomics.

Appendix A. Supplementary data

Supplementary data to this article can be found online at https://doi.org/10.1016/j.fochx.2024.102146.

Data availability

Data will be made available on request.

References

Bao, Y., & Ertbjerg, P. (2019). Effects of protein oxidation on the texture and water-holding of meat: A review. *Critical Reviews in Food Science and Nutrition, 59*(22), 3564–3578. https://doi.org/10.1080/10408398.2018.1498444

Behring, J. B., Kumar, V., Whelan, S. A., Whelan, S. A., Chauhan, P., Siwik, D. A., … Bachschmid, M. M. (2014). Does reversible cysteine oxidation link the Western diet to cardiac dysfunction? *FASEB Journal : Official Publication of the Federation of American Societies for Experimental Biology, 28*(5), 1975–1987. https://doi.org/10.1096/fj.13-233445

Decker, E. A., Xiong, Y. L., Calvert, J. T., Crum, A. D., & Blanchard, S. P. (1993). Chemical, physical, and functional properties of oxidized Turkey white muscle myofibrillar proteins. *Journal of Agricultural and Food Chemistry, 41*(2), 186–189. https://doi.org/10.1021/jf00026a007

Duan, J., Gaffrey, M. J., & Qian, W. (2017). Quantitative proteomic characterization of redox-dependent post-translational modifications on protein cysteines. *Molecular BioSystems, 13*(5), 816–829. https://doi.org/10.1039/c6mb00861e

Estevez, M., Diaz-Velasco, S., & Martinez, R. (2022). Protein carbonylation in food and nutrition: A concise update. *Amino Acids, 54*(4), 559–573. https://doi.org/10.1007/s00726-021-03085-6

Estévez, M., Kylli, P., Puolanne, E., Kivikari, R., & Heinonen, M. (2008). Fluorescence spectroscopy as a novel approach for the assessment of myofibrillar protein oxidation in oil-in-water emulsions. *Meat Science, 80*(4), 1290–1296.

Fan, X., Gao, X., Li, R., Pan, D., & Zhou, C. (2024). Myofibrillar proteins' intermolecular interaction weakening and degradation: Are they mainly responsible for the tenderization of meat containing l–arginine, l–lysine, or/and NaCl? *Food Chemistry, 441*, Article 138318. https://doi.org/10.1016/j.foodchem.2023.138318

Fu, Q., Liu, R., Zhang, W., Ben, A., & Wang, R. (2020). In vitro susceptibility of oxidized myosin by μ-calpain or caspase-3 and the determination of the oxidation sites of myosin heavy chains. *Journal of Agricultural and Food Chemistry, 68*(32), 8629–8636. https://doi.org/10.1021/acs.jafc.0c01065

Gao, S., Zhuang, S., Zhang, L., Lametsch, R., Tan, Y., Li, B., Hong, H., & Luo, Y. (2024). Proteomic evidence of protein degradation and oxidation in brined bighead carp fillets during long-term frozen storage. *Food Chemistry, 433*, Article 137312. https://doi.org/10.1016/j.foodchem.2023.137312

Gilbert, H. F. (2013). Protein modifications | disulfide bond formation. In J. Jez (Ed.), *Encyclopedia of biological chemistry III* (3rd ed., pp. 150–153). Oxford: Elsevier. https://doi.org/10.1016/B978-0-12-819460-7.00543-0.

Jia, N., Wang, L., Shao, J., Liu, D., & Kong, B. (2017). Changes in the structural and gel properties of pork myofibrillar protein induced by catechin modification. *Meat Science, 127*, 45–50. https://doi.org/10.1016/j.meatsci.2017.01.004

Jiao, X., Yan, B., Huang, J., Zhao, J., Zhang, H., Chen, W., & Fan, D. (2021). Redox proteomic analysis reveals microwave-induced oxidation modifications of Myofibrillar proteins from silver carp (Hypophthalmichthys molitrix). *Journal of Agricultural and Food Chemistry, 69*(33), 9706–9715. https://doi.org/10.1021/acs.jafc.1c03045

Jones, D. P., & Go, Y. (2011). Mapping the cysteine proteome: Analysis of redox-sensing thiols. *Current Opinion in Chemical Biology, 15*(1), 103–112. https://doi.org/10.1016/j.cbpa.2010.12.014

Lana, A., & Zolla, L. (2015). Apoptosis or autophagy, that is the question: Two ways for muscle sacrifice towards meat. *Trends in Food Science & Technology, 46*(2, Part A), 231–241. https://doi.org/10.1016/j.tifs.2015.10.001

Li, D., Tan, Z., Liu, Z., Wu, C., Liu, H., Guo, C., & Zhou, D. (2021). Effect of hydroxyl radical induced oxidation on the physicochemical and gelling properties of shrimp myofibrillar protein and its mechanism. *Food Chemistry, 351*, Article 129344. https://doi.org/10.1016/j.foodchem.2021.129344

Li, Q., Sun, X., Mubango, E., Zheng, Y., Liu, Y., Zhang, Y., Tan, Y., Luo, Y., & Hong, H. (2023). Effects of protein and lipid oxidation on the water holding capacity of different parts of bighead carp: Eye, dorsal, belly and tail muscles. *Food Chemistry, 423*, Article 136238. https://doi.org/10.1016/j.foodchem.2023.136238

Li, R., Xiong, Y. L., Subramanian, V., Suman, S. P., & True, A. D. (2024). Unlocking the gelling potential of oat protein: Synergistic effects of sonication and disulfide cleavage. *Food Hydrocolloids, 155*, Article 110241. https://doi.org/10.1016/j.foodhyd.2024.110241

Liu, J., Hu, Z., Liu, D., Zheng, A., & Ma, Q. (2023). Glutathione metabolism-mediated ferroptosis reduces water-holding capacity in beef during cold storage. *Food Chemistry, 398*, Article 133903. https://doi.org/10.1016/j.foodchem.2022.133903

Liu, J., Liu, D., Zheng, A., & Ma, Q. (2022). Haem-mediated protein oxidation affects water-holding capacity of beef during refrigerated storage. *Food Chemistry: X, 14*, Article 100304. https://doi.org/10.1016/j.fochx.2022.100304

Malheiros, J. M., Braga, C. P., Grove, R. A., Ribeiro, F. A., Calkins, C. R., Adamec, J., & Chardulo, L. A. L. (2019). Influence of oxidative damage to proteins on meat tenderness using a proteomics approach. *Meat Science, 148*, 64–71. https://doi.org/10.1016/j.meatsci.2018.08.016

Pan, D., Ma, J., Diao, J., Li, J., & Chen, H. (2023). Effects of eugenol on the structure and gelling properties of myofibrillar proteins under hydroxyl radical-induced oxidative stress. *Food Chemistry: X, 20*, Article 100946. https://doi.org/10.1016/j.fochx.2023.100946

Paulsen, C. E., & Carroll, K. S. (2013). Cysteine-mediated redox signaling: Chemistry, biology, and tools for discovery. *Chemical Reviews, 113*(7), 4633–4679. https://doi.org/10.1021/cr300163e

Qian, S., Li, X., Wang, H., Mehmood, W., Zhong, M., Zhang, C., & Blecker, C. (2019). Effects of low voltage electrostatic field thawing on the changes in physicochemical properties of myofibrillar proteins of bovine longissimus dorsi muscle. *Journal of Food Engineering, 261*, 140–149. https://doi.org/10.1016/j.jfoodeng.2019.06.013

Sanchez, R., Riddle, M., Woo, J., & Momand, J. (2008). Prediction of reversibly oxidized protein cysteine thiols using protein structure properties. *Protein Science, 17*(3), 473–481. https://doi.org/10.1110/ps.073252408

Soladoye, O. P., Juárez, M. L., Aalhus, J. L., Shand, P., & Estévez, M. (2015). Protein oxidation in processed meat: Mechanisms and potential implications on human health. *Comprehensive Reviews in Food Science and Food Safety, 14*(2), 106–122. https://doi.org/10.1111/1541-4337.12127

Xia, X., Kong, B., Liu, Q., & Liu, J. (2009). Physicochemical change and protein oxidation in porcine longissimus dorsi as influenced by different freeze–thaw cycles. *Meat Science, 83*(2), 239–245. https://doi.org/10.1016/j.meatsci.2009.05.003

Xu, C., Chen, G., Chen, S., Xu, J., Chen, C., Xia, Q., Sun, Q., Wei, S., Han, Z., Wang, Z., & Liu, S. (2024). Effect of linoleic acid-induced oxidation on the water retention of golden pompano: Myoglobin and myofibrillar protein oxidation. *LWT, 192*, Article 115719. https://doi.org/10.1016/j.lwt.2023.115719

Yu, Q., Hong, H., Liu, Y., Monto, A. R., Gao, R., & Bao, Y. (2024). Oxidation affects pH buffering capacity of myofibrillar proteins via modification of histidine residue and structure of myofibrillar proteins. *International Journal of Biological Macromolecules, 260*, Article 129532. https://doi.org/10.1016/j.ijbiomac.2024.129532

Zhang, H., Yu, X., You, J., Xiong, S., & Liu, Y. (2024). Effects of hydroxyl radicals oxidation on digestion properties of silver carp myofibrillar protein gel. *LWT, 191*, Article 115616. https://doi.org/10.1016/j.lwt.2023.115616

Zhang, L., Li, Q., Hong, H., & Luo, Y. (2021). Tracking structural modifications and oxidative status of myofibrillar proteins from silver carp (Hypophthalmichthys molitrix) fillets treated by different stunning methods and in vitro oxidizing conditions. *Food Chemistry, 365*, Article 130510. https://doi.org/10.1016/j.foodchem.2021.130510

Zhang, M., He, L., Li, C., Yang, F., Zhao, S., Liang, Y., & Jin, G. (2020). Effects of gamma ray irradiation-induced protein hydrolysis and oxidation on tenderness change of fresh pork during storage. *Meat Science, 163*, Article 108058. https://doi.org/10.1016/j.meatsci.2020.108058

Zhao, J., Cui, J., Chen, R., Tang, Z., Tan, Z., Jiang, L., & Liu, F. (2021). Real-time in-situ quantification of protein secondary structures in aqueous solution based on ATR-FTIR subtraction spectrum. *Biochemical Engineering Journal, 176*, Article 108225. https://doi.org/10.1016/j.bej.2021.108225

Zhao, J., Wang, S., Jiang, D., Chen, C., Tang, J., Tomasevic, I., & Sun, W. (2023). The influence of protein oxidation on structure, pepsin diffusion, and in vitro gastric digestion of SPI emulsion. *Food Chemistry, 428*, Article 136791. https://doi.org/10.1016/j.foodchem.2023.136791

Zhao, Z. (2023). Hydroxyl radical generations form the physiologically relevant Fenton-like reactions. *Free Radical Biology and Medicine, 208*, 510–515. https://doi.org/10.1016/j.freeradbiomed.2023.09.013